

Evaluation of residual stresses induced by cold spraying of Ti-6Al-4V on Ti-6Al-4V substrates

Boruah, D., Ahmad, B., Lee, T. L., Kabra, S., Syed, A., McNutt, P., Doré, M. & Zhang, X.

Author post-print (accepted) deposited by Coventry University's Repository

Original citation & hyperlink:

Boruah, D, Ahmad, B, Lee, TL, Kabra, S, Syed, A, McNutt, P, Doré, M & Zhang, X 2019, 'Evaluation of residual stresses induced by cold spraying of Ti-6Al-4V on Ti-6Al-4V substrates', *Surface and Coatings Technology*, vol. 374, pp. 591-602.
<https://dx.doi.org/10.1016/j.surfcoat.2019.06.028>

DOI 10.1016/j.surfcoat.2019.06.028

ISSN 0257-8972

ESSN 1879-3347

Publisher: Elsevier

NOTICE: this is the author's version of a work that was accepted for publication in *Surface and Coatings Technology*. Changes resulting from the publishing process, such as peer review, editing, corrections, structural formatting, and other quality control mechanisms may not be reflected in this document. Changes may have been made to this work since it was submitted for publication. A definitive version was subsequently published in *Surface and Coatings Technology*, [374], (2019) DOI: 10.1016/j.surfcoat.2019.06.028

© 2019, Elsevier. Licensed under the Creative Commons Attribution-NonCommercial-NoDerivatives 4.0 International

<http://creativecommons.org/licenses/by-nc-nd/4.0/>

Copyright © and Moral Rights are retained by the author(s) and/ or other copyright owners. A copy can be downloaded for personal non-commercial research or study, without prior permission or charge. This item cannot be reproduced or quoted extensively from without first obtaining permission in writing from the copyright holder(s). The content must not be changed in any way or sold commercially in any format or medium without the formal permission of the copyright holders.

This document is the author's post-print version, incorporating any revisions agreed during the peer-review process. Some differences between the published version and this version may remain and you are advised to consult the published version if you wish to cite from it.

Accepted Manuscript

Evaluation of residual stresses induced by cold spraying of Ti-6Al-4V on Ti-6Al-4V substrates



Dibakor Boruah, Bilal Ahmad, Tung Lik Lee, Saurabh Kabra, Abdul Khadar Syed, Philip McNutt, Matthew Doré, Xiang Zhang

PII: S0257-8972(19)30641-3
DOI: <https://doi.org/10.1016/j.surfcoat.2019.06.028>
Reference: SCT 24708
To appear in: *Surface & Coatings Technology*
Received date: 15 February 2019
Revised date: 23 May 2019
Accepted date: 9 June 2019

Please cite this article as: D. Boruah, B. Ahmad, T.L. Lee, et al., Evaluation of residual stresses induced by cold spraying of Ti-6Al-4V on Ti-6Al-4V substrates, *Surface & Coatings Technology*, <https://doi.org/10.1016/j.surfcoat.2019.06.028>

This is a PDF file of an unedited manuscript that has been accepted for publication. As a service to our customers we are providing this early version of the manuscript. The manuscript will undergo copyediting, typesetting, and review of the resulting proof before it is published in its final form. Please note that during the production process errors may be discovered which could affect the content, and all legal disclaimers that apply to the journal pertain.

Evaluation of residual stresses induced by cold spraying of Ti-6Al-4V on Ti-6Al-4V substrates

Dibakor Boruah^{1,2}, Bilal Ahmad¹, Tung Lik Lee³, Saurabh Kabra³, Abdul Khadar Syed¹, Philip McNutt⁴,
Matthew Doré⁵, and Xiang Zhang¹

¹ Faculty of Engineering, Environment and Computing, Coventry University, Coventry CV1 5FB, West Midlands, United Kingdom

² National Structural Integrity Research Centre (NSIRC), TWI Ltd, Cambridge CB21 6AL, Cambridgeshire, United Kingdom

³ ISIS Neutron Facility, STFC Rutherford Appleton Laboratory, Harwell Campus, Didcot OX11 0QX, Oxfordshire, United Kingdom

⁴ Surface Engineering, Materials Group, TWI Ltd, Cambridge CB21 6AL, Cambridgeshire, United Kingdom

⁵ Fatigue Integrity Management, Integrity Management Group, TWI Ltd, Cambridge CB21 6AL, Cambridgeshire, United Kingdom

*Corresponding Author: Dibakor Boruah

Email address: boruahd@uni.coventry.ac.uk | dibakor.boruah@affiliate.twi.co.uk

Phone number: +44 1223899646, +44 7423674656

Abstract

Cold spray (CS) is a solid-state additive material deposition technique, which has gained attention in the aerospace industry as a potentially viable technology for structural repair of high-value parts made of high-strength alloys such as Ti-6Al-4V (Ti-64). Residual stresses build up in the substrate and deposited materials resulting from the CS process can influence the integrity of a coating or repair. However, the nature, magnitude and distribution of residual stresses in Ti-64/Ti-64 CS repairs are currently unknown. This study aims to evaluate the effects of geometrical variables (*i.e.* the number of CS layers, CS layer thickness, and substrate thickness) and track pattern on the magnitude and distribution of residual stresses in CS deposit-substrate assemblies. Through-thickness stress distributions were measured experimentally by neutron diffraction and contour method. Furthermore, a comparison among different residual stress build-up mechanisms induced by CS processes has been discussed for different combinations of substrate and deposit assemblies. An analytical model based on the force and moment equilibrium requirements was used to

interpret the experimental stress profiles and to predict the residual stress distribution. It was found that residual stresses are highly tensile near the free surface of the Ti-64 deposits as well as towards the bottom of the substrate, and compressive near the interface region. Although all the specimens showed similar stress distribution, the magnitudes were found to be higher in one or more of the following cases: specimens with a higher number of CS layers, lower substrate thickness, higher layer thickness (*i.e.* at lower scanning speed), and deposited with a horizontal track pattern.

Keywords

Additive Manufacturing, Cold Spray, Coatings, Repairs, Residual Stress, Ti-6Al-4V

1. Introduction

Aircraft structural components are complex and expensive owing to their manufacturing process complexities and the use of high-performance materials. Titanium alloy Ti-6Al-4V (Ti-64) is used in many aircraft components (*e.g.* engine parts, load-bearing airframe, hydraulic tubing, etc.) owing to its well-known characteristics viz. high strength, high stiffness, excellent fatigue and corrosion resistance, relatively low density, etc. [1,2]. However, aerospace components are susceptible to in-service damage, such as wear, dents, corrosion pits, and cracks; caused by corrosion, fatigue loads, foreign object damage, etc. [3]. Damaged parts must be repaired or replaced to ensure continued airworthiness and high performance [4]. In most cases, repair or remanufacturing is a more desirable and economical solution than replacement. Remanufacturing of aerospace components may deliver significant cost savings between 30-70% of the cost of replacement [5]. Moreover, remanufacturing promotes sustainable manufacturing and circular economy [6].

Remanufacturing of aerospace components has become more feasible with the emergence of additive manufacturing technologies, such as the Direct Energy Deposition (DED) [4] and Cold Spray (CS) [7] processes. In CS, powder particles are deposited by means of ballistic impingement upon a substrate at supersonic velocities to form a coating. Because of the relatively lower operating temperature in the CS

process, detrimental effects arising from the high-temperature process, *e.g.* oxidation, phase transformations, compositional changes, and formation of the heat affected zones (HAZ), can be minimized or even eliminated. Furthermore, CS is highly suitable for repairing oxygen and temperature sensitive materials, such as titanium, magnesium, aluminium and copper alloys [8]. The CS technology has been proven to be an effective geometry restoration technology and has the potential to repair load-bearing structural components [9], for which structural integrity is a mandatory requirement for the durability and damage tolerance performance. In particular, the distribution and magnitude of the residual stresses built up in the substrate and deposited materials during spraying can affect the bonding strength, substrate-coating adhesion, and mechanical properties (*e.g.* fatigue and fracture performance) of a repaired part, hence the accuracy and reliability of structural integrity analysis and repair design solutions [10].

Residual stresses induced by the CS process have been investigated by many researchers for various combinations of deposit-substrate materials comprising Cu, Mg, Ti, Al and Al alloys [11]. Based on previous studies [10–14], residual stresses induced by CS processes can be classified into the peening dominant and thermal mismatch dominant mechanisms. However, there are limited literature on residual stresses induced by cold spraying of titanium and its alloys. Residual stresses in commercially pure (CP) Ti CS deposit on various substrates has been investigated: Ti on Al 6061 substrates (Ti/Al6061) using X-ray diffraction (XRD) method [15], Ti/Ti-64 using deflection method [16], Ti/Ti by means of numerical simulation [17], Ti/Cu and Ti/Fe via neutron diffraction [14]. Residual stresses in Ti-64 single splat particles were evaluated using Micro-ring-core Focused Ion Beam–Digital Image Correlation (FIB-DIC) technique and numerical simulation [18]. So far, cold spraying of Ti-64 alloy received significant attention by many researchers, in terms of microstructure and mechanical properties [19–22], tribological and corrosion properties [23–28], and influence of CS process conditions on various aspects of deposited material [29–32]. In addition, the effect of powder processing and powder characteristics [29,33–39], substrate surface conditions [40], and post-deposition thermal treatments [35,36,41–45] on the coating characteristics are also investigated. However, there is no published work in open literature available on the through-thickness distribution of residual stresses for CS Ti-64 deposited on a Ti-64 substrate. Therefore, the nature, magnitude and through-

thickness distribution of residual stresses in Ti-64 deposits on Ti-64 substrate by cold spraying is not well understood.

In the present study, residual stresses induced by cold spraying of Ti-64 on Ti-64 substrate was firstly evaluated by the neutron diffraction method and the contour method. An analytical model was then used to interpret the experimental results and to study different mechanisms for residual stress generation, namely the peening dominant, thermal mismatch dominant, and high thermal gradient and quenching dominant CS processes. Finally, a parametric study was carried out on the effect of geometrical variables, scanning speed and track pattern on the distribution and magnitude of residual stresses.

2. Materials and experiments

2.1 Feedstock powder and substrate material

The current study used commercially available gas atomised Ti-64 powder (Grade 5, nominal size 15-32 μ m), provided by LPW Technology Ltd., Cheshire, UK. The substrate material used in this study was Mill Annealed Ti-64 (Grade 5) supplied by Dynamic Metals Ltd, Bedfordshire, UK. Table I lists the chemical composition of the powder and substrate material. Figure 1 shows the particle size distribution, powder morphology, and microstructure predominantly consisting of hexagonal close-packed martensitic α' phase. Characteristics of Ti-64 powders used for CS can be found in [21,33,36].

2.2 Specimen preparation and characterisation

All specimens were manufactured using an Impact Innovation 5/11 CS System at TWI Ltd, Cambridge, UK. Key process parameters used for CS are shown in Table II. Six specimens were produced for residual stress measurements, as listed in Table III. Prior to residual stress measurements, the cross-section of a specimen (identical to the specimens listed in Table III) parallel to the spraying direction was characterised in terms of porosity and microstructure by following standard metallographic preparation and examination techniques. Porosity in the CS deposited material was found to be $2.69 \pm 0.28\%$, measured using image analyses software ImageJ as per ASTM E2109 [46]. , (b) cross-hatch track pattern

Figure 3 shows the SEM microstructure of the cross-sectioned specimen. Two distinctive regions were observed in the CS deposits: (i) undeformed ‘textured’ regions, and (ii) severely deformed ‘smooth’ regions, as also found by other researchers [19–21]. Details of the microstructure evolution in CS Ti-64 can be found in [19,21].

2.3 Residual stress evaluation methods

2.3.1 Neutron diffraction

Neutron diffraction measurements were performed at ENGIN-X time-of-flight neutron diffractometer at the ISIS pulsed neutron facility, Rutherford Appleton Laboratory, Harwell Campus, UK [47]. The residual stress measurements were performed in a CS deposit-substrate coupon (Ti-64/Ti-64) of size $9.5 \times 30 \times 60 \text{ mm}^3$ as shown in Figure 4 (a). The measurements were performed at the mid-length of the specimen in the thickness direction, from the bottom of the substrate progressing towards the interface, and then from the top of the CS deposits progressing towards the interface. A cuboid gauge volume of $1 \times 1 \times 15 \text{ mm}^3$ (defined by the slit dimensions and the position of the bank collimators) was used for all measurements. No in-plane variation in strains was expected along either of these directions owing to the symmetry of the deposition process. The longest dimension of the gauge volume was along the length (60 mm) or the width (30 mm) of the specimen, in order to increase the counting statistics and reduce the counting time.

Lattice parameters of multiple crystallographic planes were measured at once at a fixed angle using a white beam of neutrons with a range of wavelengths close to atomic distances. The time of flight technique allows the counting of neutrons diffracted by multiple planes simultaneously [48,49]. Initially, measurements were performed in the two orthogonal directions (longitudinal (Z) and normal (X)) simultaneously, using the two detector banks (bank 1 and bank 2) positioned at a Bragg's angle of $\pm 90^\circ$ (as shown in Figure 4 (c)). The specimen was repositioned to measure the third direction *i.e.* the transverse direction (Y). As a result, the lattice parameters in the normal direction were obtained twice. Overall, nine measurements were performed in the specimen, five measurements in the CS deposits (4.5 mm thick), and four measurements in the substrate (5mm thick), in two orientations a total of 18 (9×2) measurements were performed for the as-

sprayed deposit-substrate coupon. No measurements were performed at the interface as the positioning the gauge volume is challenging at the deposit-substrate interface.

Stress-free lattice parameters ($d_{hkl,0}$) were measured in a stress-free specimen of dimension $3 \times 3 \times 7.5$ mm³ for both CS deposits and the substrate material, as shown in Figure 4 (b). This specimen was extracted from the centre of a specimen of size $7.5 \times 20 \times 30$ mm³ using wire electro-discharge machining (WEDM) to mechanically relieve the residual stresses. A gauge volume of $1 \times 1 \times 3$ mm³ was used for the stress-free measurements, in two orientations a total of 4 (2×2) measurements were performed.

Eleven planes were identified in the hexagonal-close-packed (HCP) α , within the analysed time-of-flight (TOF) ranged between 20,000 μ s and 47,500 μ s. They were fitted in whole using Pawley refinement [50] to determine the plane spacing ' d_{hkl} ' values (*i.e.* the spacing between adjacent hkl lattice planes). HCP metals are notoriously anisotropic, hence choosing the right reflection is the key. The crystallographic plane $\{10\bar{1}1\}$ was found to be very consistent in terms of providing good signal strength/intensity with minimal fitting errors in each orientation for both substrate and the CS deposits. Similar observations were reported in [48,49,51] for Ti-64 alloy, and $\{10\bar{1}1\}$ diffraction peak was used for residual stress calculations. Figure 5 shows exemplary fitted spectra from a measurement point in the CS region for longitudinal, normal, and transverse directions. Lattice strain (ϵ) and residual stress (σ) in the three principal directions (longitudinal, transverse and normal) were calculated based on the ' d_{hkl} ' values from the crystallographic plane $\{10\bar{1}1\}$, using Eq. (1), and (2), respectively [48]. For these calculations, a Young's modulus (E) value of 98 MPa [52] was used which is specific to the crystallographic plane $\{10\bar{1}1\}$, and a Poisson's ratio of 0.34 [48,53].

$$\epsilon = \frac{d_{hkl} - d_{hkl,0}}{d_{hkl,0}} \quad (1)$$

$$\sigma_{ii} = \frac{\nu_{hkl} E_{hkl}}{(1 + \nu_{hkl})(1 - 2\nu_{hkl})} (\epsilon_{xx} + \epsilon_{yy} + \epsilon_{zz}) + \frac{E_{hkl}}{1 + \nu_{hkl}} \epsilon_{ii} \quad (2)$$

Since Ti is a weak coherent and high incoherent neutron scatterer, it took longer time for a peak acquisition. For the CS deposits, it took ~3.5 hours, and for the substrate material, it took ~3 hours for a peak acquisition using the gauge volume of $1 \times 1 \times 15$ mm³. A total of 22 points (18+4) were measured in three days, including

experimental set-up time. Therefore, it was possible to measure stresses only in one specimen due to the limited time available at the ISIS facility.

2.3.2 Contour method

After the non-destructive neutron diffraction measurements at the ISIS facility, the contour method [54] was used to perform further investigation. Contour method is a destructive technique for residual stress measurement, and is based on the stress relaxation, where a part is cut into two halves, and the stress component being measured is normal to the cut surface [54]. Using the contour method, a parametric study was performed to examine the effect of geometrical variables (*i.e.* number of CS layers, CS layer thickness, and substrate thickness), and track pattern on the magnitude and distribution of residual stresses in CS deposit-substrate coupons in five different conditions and a substrate only specimen, as presented in the Table III. As shown in Figure 6 (specimen CS2 from Table III as an example), specimens were cut into two halves using a Fancu Robocut α -C600i wire electro-discharge machine (WEDM), using a 0.25 mm diameter brass wire. The sample was simultaneously cut through the CS deposits and the substrate material. Specimens were clamped rigidly during the cutting process to avoid any free movement during the cutting process. WEDM low power cutting parameters (*i.e.* selection of low values for important electrical parameters [55]) were used for the sample material and thickness. Also, a higher value for the electrical spark OFF time was set to improve flushing of the removed/cut material. The WEDM cut progressed smoothly without wire breakage and any significant variation in the cutting speed. The cutting speed of all samples was set at 0.5 mm/min.

The relaxed deformation profiles of the cut surfaces were measured using a Zeiss Contura g2 coordinate measuring machine (CMM) with a 0.5 mm diameter touch trigger probe. The distance from the perimeter and between the individual measurement points in both directions of the sample surface was set as 0.1 mm. The displacement data of both cut surfaces of each sample was post-processed for data aligning, cleaning, flattening and smoothing using the Matlab analysis routines. The data smoothing of all samples (with exception of sample CS6) was performed with a cubic spline knot spacing of 2.5 mm along X-direction and 3.5 mm along Y-direction. The spline knot spacing was selected on the basis of the good fit of the averaged

displacement data. For sample CS6 a coarser spline knot spacing of 8 mm was used in both X and Y directions.

The original out-of-plane residual stress field at the cut surfaces were back-calculated by applying the smoothed CMM profile as a boundary condition in a 3D linear elastic finite element (FE) model of one cut half of the samples. An 8-node brick element (C3D8R) was selected in the ABAQUS software. The non-uniform mesh size was used on the cut surface, and this distance was in the range of 0.1-0.5 mm for all samples. In the linear elastic FE model, different elastic properties were used. Young's modulus (E) values for both the material (mill annealed Ti-64 substrate and the CS Ti-64 deposits) were measured by Impulse Excitation technique as per ASTM E1876–15 [56], assuming Poisson's ratio as 0.34 [48,53]. This method has also been used by other researchers for CS deposits [10,12,13]. Rectangular specimens of size $6 \times 20 \times 110$ mm³ were used for each measurement. Figure 7 shows the set-up of the impulse excitation measurements. From the impulse excitation test, Young's modulus (E) values were found as 113.32 ± 0.12 GPa (mill annealed Ti-64, substrate material) and 88.45 ± 0.04 GPa (CS Ti-64, deposited material).

In order to compare residual stress profiles among the specimens, stress values were extracted from the central 15 mm region of the contour cut surface (X-Y plane) by creating 15 different paths along the X-direction. The averaged values were used for comparison among the specimens, to study the effect of geometrical variables and track pattern on the distribution and magnitude of residual stresses. Averaging stress values over the central 15 mm region resulting from the contour method also facilitated comparison with neutron diffraction results that uses a gauge volume of $1 \times 1 \times 15$ mm³.

3. Results and discussion

3.1 Neutron diffraction

Figure 8 shows the through-thickness residual stress distribution of specimen CS1 in the normal (X), transverse (Y), and longitudinal (Z) directions. It can be seen that all three stress components are highly tensile in nature just below the free surface of the Ti-64 deposits; the highest stress magnitude is in the longitudinal direction reaching 355 MPa, gradually becomes compressive towards the interface. In the

longitudinal direction, the maximum compressive stress is around 249 MPa (highest among the three directions), gradually changing to tensile towards the bottom of the substrate reaching 100 MPa. The stress uncertainty values were calculated based on the fitting errors for the measured diffraction peaks, which were found to be within the range of ± 49.83 to ± 56.26 for the substrate material, and ± 57.67 MPa to ± 64.10 MPa for the deposited material, as represented by the error bars in Figure 8. Along the thickness direction, the two in-plane stress components (longitudinal and transverse) are very similar without significant variations in the stress distribution and the order of magnitude, which was expected due to the symmetry of the deposition process. In CS, the stress state in the coating is usually equal-biaxial, due to the presence of in-plane symmetry resulting from spraying particles impacting perpendicular to the surface [14].

3.2 Parametric study by contour method

Two dimensional (2D) residual stress maps produced by the contour method on the X-Y plane (longitudinal stress component) for all six specimens (CS1-CS6) are shown in Figure 9 (a). Specimen CS6 shows the stress state in a substrate prior to CS deposition. For all the CS deposited specimens (CS1-CS5), it was found that residual stresses near the free surface of the CS deposits are tensile in nature reaching 348 MPa, 95 MPa, 77 MPa, 173 MPa, and 101 MPa, respectively, for specimens CS1, CS2, CS3, CS4, and CS5. Large compressive residual stresses can be seen just below the interface reaching 262 MPa, 73 MPa, 58 MPa, 83 MPa, and 67 MPa, respectively, for specimens CS1, CS2, CS3, CS4, and CS5. To balance the stresses within the system, it becomes gradually tensile towards the bottom of the substrate, however, the magnitudes are lower than the CS deposits. Moreover, balancing compressive stress regions were observed at the side edges (especially significant for specimens CS2 and CS5) and the bottom of the substrate.

Figure 9(b-d) shows the effect of geometrical variances (layer thickness, substrate thickness and total deposition thickness), and track pattern on residual stress distribution. Residual stress profiles presented in Figure 9(b-d) were extracted from the results of the contour method, which were averaged over the central 15 mm length region of the contour cut surface. The error bar shows the standard deviation over the 15 mm length region.

Figure 9(b) compares residual stress distributions in specimens CS1 and CS2 having different numbers of CS layers. It was found that both the tensile and compressive residual stresses are much lower in specimen CS2 (14 CS layers, 1.5 mm deposition thickness) as compared to specimen CS1 (42 CS layers, 4.5 mm deposition thickness). However, the trend of stress distribution is similar in both the cases, *i.e.* tensile residual stresses are at the top and bottom of the specimen, and compressive stresses are near the interface.

Figure 9(c) compares specimens CS2, CS3 and CS4, showing the effect of average layer thickness (layer thickness is directly linked with the scanning speed, see Table III) and track pattern on residual stresses. It was found that specimen CS4 with a higher individual layer thickness ($\sim 187\mu\text{m}$) had higher tensile residual stresses in the CS deposited material compared to specimen CS2 with layer thickness $\sim 107\mu\text{m}$. Moreover, compressive residual stresses just below the interface are higher in CS4 than that of CS2. In addition, specimen CS3 deposited with cross-hatch track pattern had lower tensile residual stress in the CS deposits and also lower compressive stress just below the interface compared with specimen CS2 with horizontal track pattern.

Figure 9(d) shows the effect of substrate thickness by comparing specimen CS2 (5 mm substrate thickness) with CS5 (10 mm substrate thickness). It was found that CS2 with lower substrate thickness had higher compressive residual stresses near the interface and higher tensile residual stresses in the CS deposits as well as in the substrate. Similar findings on the effect of substrate thickness and number of deposited layer were also reported in the literature for the CS process [11], and the selective laser melting (SLM) process [57,58].

4. Discussion

4.1 Comparison and contrast among different residual stress mechanisms

It is known from the literature [11,14] that residual stresses induced by the CS processes can be categorised into two different mechanisms: (i) peening dominant CS process (Type A in Table IV), and (ii) thermal mismatch dominant CS process (Type B in Table IV). These two mechanisms were thoroughly discussed in [11]. In the peening dominant process, the peening stresses originating from the plastic deformation caused by constant bombarding of the high-velocity spraying particles are dominant over thermally induced stresses.

The reduced thermal input in the peening dominant process is due to the use of lower deposition temperature and pressure, and the negligible difference in the coefficients of thermal expansion between the deposited and substrate materials. Table IV (image 'a') shows a peening dominant residual stress profile, where residual stresses are compressive both at the top side of CS deposits and towards the bottom of the substrate, and tensile at the interface [11–13,59]. On the other hand, the thermal mismatch dominant CS processes (Type B) uses moderate deposition temperature and pressure. Therefore, the thermal stresses are dominant, owing to the different thermal contraction of the substrate and deposited material, which is significant if there is a considerable difference in the coefficients of thermal expansion between the substrate and CS deposited material. Table IV (image 'b') shows a thermal mismatch dominant residual stress profile, where residual stresses are tensile near the free surface of the CS deposits and also in the substrate side of the interface. Compressive residual stress is towards the bottom of the substrate and in the CS deposits just above the interface [11,13,14].

The critical temperature or pressure, above which a process will behave as thermal mismatch dominant rather than peening dominant, is currently unknown. A low-temperature process may also behave thermal mismatch dominant if there is a huge difference in the thermal expansivities between the deposited and substrate material. Moreover, materials having similar thermal expansivities may behave differently in different spraying conditions. For example: the stress profile of Al/Mg was found to be peening dominant when sprayed at a temperature range of 77-217°C using He as a process gas, and thermal mismatch dominant when sprayed at 550°C using N₂ as a process gas [13]. Moreover, in the case of Ti/Cu, stress profile was found to be thermal mismatch dominant, which is due to (i) difference in the thermal expansion coefficient of Cu and Ti, and (ii) use of moderate/higher temperature (615°C using N₂ as a process gas, and 365°C using He as process gas) [14]. However, which one has more contribution towards the final residual stress state is currently unknown (use of high temperature, or differences in thermal expansivities). In addition to the process parameter, the coating thickness and its geometry of the substrate plays a vital role in defining the overall residual stresses in a CS deposit-substrate assembly. For high-temperature and high-pressure CS

process, through-thickness residual stresses profile of IN718/IN718 (sprayed using N_2 at $950^\circ C$) reported in [60] was different from typical CS and/or thermal spray processes reported in [11–14,61]; which might be owing to the difference in specimen geometry, as cylindrical specimens were investigated in [60] for very thin coatings (613-730 μm), whereas rectangular specimens (1.0-4.7 mm coating thickness) were stated in [11–14,61].

In this study, CS Ti-64/Ti-64 deposit-substrate coupons were deposited using N_2 as process gas at a very high temperature and pressure ($1100^\circ C$, 5 MPa). From the stress profiles determined by neutron diffraction and contour method, it was found that stresses are highly tensile near the free surface of the CS deposits and towards the bottom of the substrate, and highly compressive near the interface, as shown by image 'c' in Table IV (Type C). Residual stresses build-up during cold spraying Ti-64 on Ti-64 substrates is mainly caused by: (i) quenching stresses arising from the contraction of the individual cold sprayed splats as they rapidly cool down to the substrate temperature, which is always tensile in nature; (ii) macroscopic differential thermal contraction stresses arising when both the substrate and deposited material (having a high thermal gradient as a result of the multi-pass deposition process at high temperature) cool down together, resulting in differential thermal contraction/shrinkage in the free surfaces and the core of the deposit-substrate assembly [62]. Since, both the substrate and deposited materials are the same, there is no difference between the coefficients of thermal expansion. The distribution of residual stresses in CS Ti-64/Ti-64 deposit-substrate coupons can be compared to the stress distribution in the thermally dominant processes, such as Plasma Sprayed Al on Al substrate [14], Wire and Arc Additive Manufactured Ti-64 on Ti-64 substrate [53], Selective Laser Melted/Sintered steel on similar substrates [57,63].

4.2 Analytical prediction

Based on the aforementioned stress distribution for Ti-64/Ti-64 from experimental measurements, the stress build-up mechanism during CS can be explained with the help a conceptual model based on the force and moment equilibrium requirements within a deposit-substrate assembly. The original idea of this model was taken from Shiomi et al. [63], which was further developed for the SLM process [57], and CS processes

(peening dominant, and thermal mismatch dominant, *i.e.* Type A and Type B in Table IV) [11]. raged stresses in the X-Y plane for comparison among the specimens.

Figure 10 shows the residual stress build-up mechanism in high thermal gradient and quenching dominant CS process (Type C from Table IV) due to deposition of the one, two, three, and n^{th} layer, respectively; which demonstrates the redistribution of residual stresses within the substrate and previously deposited CS layers due to the stresses induced by a newly deposited layer. This mechanism is similar to the SLM process as reported in [57,58,63]. For the analytical prediction of stress distribution in the case of CS Ti-64/Ti-64, the substrate was presumed to be free from residual stresses prior to spraying, as found from the contour results (Figure 9). It was assumed that residual stresses in a newly deposited layer or near the free surface had a value ‘ k ’, which was tensile in nature and constant throughout the layer thickness (Δh) [11,57]. Owing to the deposition of a new CS layer, a linear increment of residual stresses in the substrate was assumed (Figure 10), governed by the equation ($\Delta\sigma_n(H) = a_n H + b_n$) [11,57]. After solving the values of (a_n, b_n) using the force and moment equilibrium equations (see [11] for detailed mathematical derivation), the total increment of residual stresses in the substrate due to the deposition of ‘ n ’ layers of CS can be expressed by eq. (3). The total stress increment in the $1^{\text{st}}, 2^{\text{nd}}, \dots, (n-1)^{\text{th}}$ layers, respectively, due to the deposition of the n^{th} CS layer can be expressed by eq. (4) [11,57].

$$\Delta\sigma_{TS(nL)}(H) = -6kH\Delta h \sum_{n=1}^n \left\{ \frac{h+n\Delta h}{\{h+(n-1)\Delta h\}^3} \right\} + k\Delta h \sum_{n=1}^n \left\{ \frac{2h+(2n+1)\Delta h}{\{h+(n-1)\Delta h\}^2} \right\} \quad (3)$$

$$\Delta\sigma_{T(Lm)(Ln)}(H) = k - 6kH\Delta h \sum_{m+1}^n \left\{ \frac{h+n\Delta h}{\{h+(n-1)\Delta h\}^3} \right\} + k\Delta h \sum_{m+1}^n \left\{ \frac{2h+(2n+1)\Delta h}{\{h+(n-1)\Delta h\}^2} \right\} \quad (4)$$

where, a_n and b_n are constants related to the material, process parameter and geometry, h is the substrate thickness, Δh is the average layer thickness, H is the distance from substrate bottom surface, k is the residual stress value in a newly deposited CS layer or near the free surface, n is the number of CS layers (1, 2, 3, ... n), m represents each individual CS layer below the n^{th} layer (*i.e.* $m = 1, 2, 3, \dots, (n-1)$), $\Delta\sigma_{TS(nL)}(H)$ is the total (T) stress increment in the substrate (S) due to deposition of ‘ n ’ layers (nL), and

$\Delta\sigma_{T(Lm)(Ln)}(H)$ is the total (T) stress increment in m^{th} layer (Lm) due to deposition of the n^{th} layer (Ln) [11,57].

For the analytical prediction of residual stresses in specimen CS1, the ‘ k ’ value in the eqs. (3,4) was set as 200MPa based on the experimental results by the contour method. Other parameters used for calculations are based on Table III, *i.e.* $h = 5$ mm, $\Delta h = 107$ μ m, $n = 42$, $m = 1, 2, 3, 4, \dots, 41$, and H varies from 0 to 9.5mm. A comparison of analytical predictions with the experimental results is presented in section 4.3 below.

4.3 Comparison of neutron diffraction, contour method and analytical prediction

Figure 11 shows the comparison among the experimental results (measured by neutron diffraction and contour method) and the analytical predictions for specimen CS1. Good agreement was achieved among the experimental measurements and predicted results, apart from two points in the CS deposited material, *i.e.* at 0.9 mm and 3.6 mm distance from the free surface of the deposited material, measured by neutron diffraction. The considerable difference at these two points might be due to two reasons. Firstly, the neutron diffraction results are specific to the crystallographic plane $\{10\bar{1}1\}$ which will be influenced by the localised hardening and crystallographic texture in the material, particularly at the interface. On the other hand, residual stress calculations by contour method is based on displacements in the cut surface and did not account for any variation in the crystallographic texture. Secondly, Young’s modulus (E) used in both neutron diffraction and contour methods have different values. Moreover, there are limited neutron data points to perform a good comparison with the contour results; and it was not possible to measure more points within a 9.5 mm thick specimen without overlapping the gauge volumes while using a 1 mm radial collimator. Although, the smallest radial collimator available at the ENGIN-X facility is 0.5 mm, it was not be used, as the counting time will not be feasible for Ti alloys. Furthermore, the considerable process induced defects (Figure 3a) may deteriorate the WEDM cut surface by creating outliers, which may have affected the displacement profile captured via CMM. Although the outlier data points in CMM were removed during analysis, however, the influence of it can still affect the overall stress distribution and

magnitude. In addition, the differences between experimental measurements and predicted values could also be due to the inhomogeneity in the deposited material, or assumptions of the analytical model.

4.4 Influence on the mechanical properties

The CS process is known for introducing beneficial compressive residual stresses in both deposited material and the substrate resulting from the peening impact of the sprayed particles [64–66]. Many researchers have reported a significant increase in fatigue performance (by 9-30%) in CS coated specimens (*e.g.* Mg and Al alloys) due to the presence of compressive residual stresses in the coating, as it reduces the effective applied stress and retards crack initiation and propagation [65,67,68]. The high cycle fatigue performance of Al-Si alloy was reported to be increased by >200% after applying Al-SiC composite coating by CS [69]. Moreover, it is hypothesized that compressive residual stresses may also contribute towards the increased coating-substrate adhesion strength [70].

However, in the case of Ti-64 deposited on Ti-64 substrates, high tensile residual stresses were found near the free surface of the coating and towards the bottom of the substrate. Presence of high tensile residual stresses in CS Ti-64/Ti-64 deposit-substrate assemblies in conjunction with external tensile cyclic loading will increase the mean stress. Moreover, stresses are much higher at the surfaces if a part experiences bending loads resulting in substantially higher stresses in the outmost regions. Therefore, the presence of tensile stresses at the exposed surfaces may encourage crack initiation and rapid propagation leading to reduced fatigue life and load carrying capacity of a repaired part or a coated component [71]. Also, when an external load is applied to a component, redistribution of residual stresses may occur depending on the magnitude of external load and geometry of the component. Further investigation is required to study the materials behaviour and redistribution of residual stresses within a CS Ti-64/Ti-64 component/specimen due to the application fatigue loading. Reduction in fatigue life (9-15%) after cold spraying of Ti on Ti-64 substrates was reported in [16,72], which might be due to the variation occurred in the substrate surface topography and the presence of tensile residual stresses within the substrate. Furthermore, the presence of tensile residual stresses in the coating will increase the tendency of debonding or delamination at the

coating-substrate interface, especially for thicker coatings. The build-up of tensile residual stresses in the coating during the deposition process limits the maximum coating thickness that can be achieved [73]. In the case of CS Ti-64/Ti-64, residual stresses increased with the increase in coating thickness. In fact, the coating generally starts to delaminate from the substrate after achieving a certain thickness of around 5-6 mm. In addition, development of high residual stresses during the deposition of Ti-64 on Ti-64 may lead to undesirable deformation/distortion in a component, as a result of redistribution of residual stresses to find a new equilibrium. Therefore, more research is required in this area to understand the influence of process induced residual stresses on the mechanical performance of a Ti-64 component repaired by cold spraying of Ti-64.

5. Conclusions

In this study, the through-thickness distribution of residual stress in cold spray (CS) deposit-substrate coupons (Ti-64 on Ti-64) was evaluated experimentally using the neutron diffraction and contour method. A parametric study was performed using the contour method to study the effect of geometrical variables (*i.e.* layer thickness, number of deposited layers, and substrate thickness) and deposition track patterns on the distribution and magnitude of residual stresses. Furthermore, stress development mechanism during cold spraying of Ti-64 on a Ti-64 substrate was interpreted and compared with different residual stress build-up mechanisms for various combination of metal and alloys. Predictions were made using an analytical model based on the equilibrium requirement of the force and moment resulting from the residual stresses. The following conclusions can be drawn based on this study:

1. Residual stresses were found to be highly tensile in nature near the free surface of the Ti-64 deposits and towards the bottom of the substrate. Substantial compressive residual stresses were found near the interface region. Due to the use of higher deposition temperature (1100 °C), residual stresses arising from high thermal gradient and quenching were dominant over the peening stresses. Good agreement was generally achieved among the neutron diffraction, contour method and analytical predictions.

2. All specimens showed a similar trend of residuals stress distribution. However, the magnitude of residual stresses were lower for one or more of the following cases: fewer deposited layers, lower layer thickness (*i.e.* at higher scanning speed), higher substrate thickness, and using the cross-hatch deposition track pattern.
3. Among all the investigated specimens, the highest tensile stress (peak value within the specimen) was found to be 349 MPa using the contour method (355 MPa via neutron diffraction) for the CS specimen having 42 layers (4.5 mm deposition thickness) deposited with horizontal track pattern. The lowest tensile stress (peak value) was recorded as 77 MPa using the contour method in a specimen having 14 layers (1.5 mm deposition thickness) deposited with cross-hatch track pattern.

Acknowledgements

This publication was made possible by the sponsorship and support of the Lloyd's Register Foundation, which is a charitable organization that helps to protect life and property by supporting engineering-related education, public engagement and the application of research. Coventry University has also contributed to the PhD studentship. Authors would like to thank Dr Hua Guo from Coventry University for performing the CMM measurements, Jazeel Rahman Chukkan from TWI Ltd for helping with the neutron diffraction measurements, and Dr Andreu Laborda from TWI Ltd for some useful discussions.

References

- [1] I. Inagaki, T. Takechi, Y. Shirai, N. Ariyasu, Application and Features of Titanium for the Aerospace Industry, Shimaya, Konohana-ku, Osaka, Japan, 2014.
- [2] R.R. Boyer, An overview on the use of titanium in the aerospace industry, Mater. Sci. Eng. A. 213 (1996) 103–114.
- [3] W. Sun, A.W.Y. Tan, I. Marinescu, E. Liu, Effects of Surface Roughness on Bonding Behavior of Cold Spray Ti6Al4V Coatings, in: Proc. ASME 2017 12th Int. Manuf. Sci. Eng. Conf., Los Angeles, CA, USA, June 4-8, 2017: pp. 1–6.
- [4] R. Liu, Z. Wang, T. Sparks, F. Liou, J. Newkirk, Aerospace component repair with additive manufacturing, in: Laser Addit. Manuf., Elsevier Ltd, 2017: pp. 361–371.

- [5] R. Cottam, V. Luzin, Q. Liu, N. Mathews, Y. Wong, M. Brandt, Stress Relief Heat Treatment for Laser Cladding Repair of Ti-6Al-4V Aircraft Components, in: AIAC15 15th Aust. Int. Aerosp. Congr., 2013.
- [6] B. Sheerman, C. Spelman, Tripple Win: The Social, Economic and Environmental Case for Remanufacturing, 2014. <http://www.remanufacturing.org.uk/pdf/story/2p650.pdf>.
- [7] H. Assadi, H. Kreye, F. Gärtner, T. Klassen, Cold spraying – A materials perspective, *Acta Mater.* 116 (2016) 382–407.
- [8] T. Suhonen, T. Varis, S. Dosta, M. Torrell, J.M. Guilemany, Residual stress development in cold sprayed Al, Cu and Ti coatings, *Acta Mater.* 61 (2013) 6329–6337.
- [9] R. Jones, L. Molent, S. Barter, N. Matthews, D. Tamboli, Supersonic particle deposition as a means for enhancing the structural integrity of aircraft structures, *Int. J. Fatigue.* 68 (2014) 260–268.
- [10] M. Saleh, V. Luzin, K. Spencer, Analysis of the residual stress and bonding mechanism in the cold spray technique using experimental and numerical methods, *Surf. Coatings Technol.* 252 (2014) 15–28.
- [11] D. Boruah, X. Zhang, M. Doré, Theoretical prediction of residual stresses induced by cold spray with experimental validation, *Multidiscip. Model. Mater. Struct.* 15 (2019) 599–616.
- [12] V. Luzin, K. Spencer, M.X. Zhang, Residual stress and thermo-mechanical properties of cold spray metal coatings, *Acta Mater.* 59 (2011) 1259–1270.
- [13] K. Spencer, V. Luzin, N. Matthews, M.X. Zhang, Residual stresses in cold spray Al coatings: The effect of alloying and of process parameters, *Surf. Coatings Technol.* 206 (2012) 4249–4255.
- [14] V. Luzin, K. Spencer, M. Zhang, N. Matthews, J. Davis, M. Saleh, Residual Stresses in Cold Spray Coatings, in: P. Cavaliere (Ed.), *Cold -Spray Coatings*, Springer, Cham, 2018: pp. 451–480.
- [15] S. Gulizia, A. Trentin, S. Vezzù, S. Rech, M. Jahedi, M. Guagliano, Characterisation of cold spray titanium coatings, *Mater. Sci. Forum.* 654–625 (2010) 898–901.
- [16] T.S. Price, P.H. Shipway, D.G. McCartney, Effect of Cold Spray Deposition of a Titanium Coating on Fatigue Behavior of a Titanium Alloy, *J. Therm. Spray Technol.* 15 (2006) 507–512.
- [17] T.-D. Phan, S. Masood, M. Jahedi, S. Zahiri, Residual stresses in cold spray process using finite element analysis, *Mater. Sci. Forum.* 654–656 (2010) 1642–1645.
- [18] X. Song, J. Everaerts, W. Zhai, H. Zheng, A.W.Y. Tan, W. Sun, F. Li, I. Marinescu, E. Liu, A.M. Korsunsky, Residual stresses in single particle splat of metal cold spray process – Numerical simulation and direct measurement, *Mater. Lett.* 230 (2018) 152–156.
- [19] A.M. Birt, V.K. Champagne, R.D. Sisson, D. Apelian, Microstructural Analysis of Cold-Sprayed Ti-6Al-4V at the Micro- and Nano-Scale, *J. Therm. Spray Technol.* 24 (2015) 1277–1288.

- [20] A.W.Y. Tan, W. Sun, A. Bhowmik, J.Y. Lek, I. Marinescu, F. Li, N.W. Khun, Z. Dong, E. Liu, Effect of coating thickness on microstructure, mechanical properties and fracture behaviour of cold sprayed Ti6Al4V coatings on Ti6Al4V substrates, *Surf. Coatings Technol.* 349 (2018) 303–317.
- [21] J.Y. Lek, A. Bhowmik, A.W.Y. Tan, W. Sun, X. Song, W. Zhai, P.J. Buenconsejo, F. Li, E. Liu, Y.M. Lam, C.B. Boothroyd, Understanding the microstructural evolution of cold sprayed Ti-6Al-4V coatings on Ti-6Al-4V substrates, *Appl. Surf. Sci.* 459 (2018) 492–504.
- [22] M.V. Vidaller, A. List, F. Gaertner, T. Klassen, S. Dosta, J.M. Guilemany, Single Impact Bonding of Cold Sprayed Ti-6Al-4V Powders on Different Substrates, *J. Therm. Spray Technol.* 24 (2015) 644–658.
- [23] N.W. Khun, A.W.Y. Tan, K.J.W. Bi, E. Liu, Effects of working gas on wear and corrosion resistances of cold sprayed Ti-6Al-4V coatings, *Surf. Coatings Technol.* 302 (2016) 1–12.
- [24] M.Á. Garrido, P. Sirvent, D. Elvira, Á. Rico, C.J. Múnez, P. Poza, Response of Cold Sprayed Ti6Al4V Coatings to Solid Particle Erosion and Micro-Scratch Wear Processes, *Mater. Sci. Forum.* 941 (2018) 1680–1685.
- [25] V.N.V. Munagala, T.B. Torgerson, T.W. Scharf, R.R. Chromik, High temperature friction and wear behavior of cold-sprayed Ti6Al4V and Ti6Al4V-TiC composite coatings, *Wear.* 426–427 (2019) 357–369.
- [26] P. Poza, P. Sirvent, Á. Rico, C.J. Múnez, M.Á. Garrido, Oscillating Contact Wear in Cold Sprayed Ti6Al4V Coatings for Aeronautical Repairs, *Mater. Sci. Forum.* 941 (2018) 1686–1691.
- [27] W. Sun, A.W.Y. Tan, I. Marinescu, W.Q. Toh, E. Liu, Adhesion, tribological and corrosion properties of cold-sprayed CoCrMo and Ti6Al4V coatings on 6061-T651 Al alloy, *Surf. Coatings Technol.* 326 (2017) 291–298.
- [28] N.W. Khun, A.W.Y. Tan, W. Sun, E. Liu, Wear and Corrosion Resistance of Thick Ti-6Al-4V Coating Deposited on Ti-6Al-4V Substrate via High-Pressure Cold Spray, *J. Therm. Spray Technol.* (2017).
- [29] V.S. Bhattiprolu, K.W. Johnson, O.C. Ozdemir, G.A. Crawford, Influence of feedstock powder and cold spray processing parameters on microstructure and mechanical properties of Ti-6Al-4V cold spray depositions, *Surf. Coatings Technol.* 335 (2018) 1–12.
- [30] D. Goldbaum, J.M. Shockley, R.R. Chromik, A. Rezaeian, S. Yue, J.G. Legoux, E. Irissou, The effect of deposition conditions on adhesion strength of Ti and Ti6Al4V cold spray splats, *J. Therm. Spray Technol.* 21 (2012) 288–303.
- [31] A.W.Y. Tan, W. Sun, Y.P. Phang, M. Dai, I. Marinescu, Z. Dong, E. Liu, Effects of Traverse Scanning Speed of Spray Nozzle on the Microstructure and Mechanical Properties of Cold-Sprayed Ti6Al4V Coatings, *J. Therm. Spray Technol.* 26 (2017) 1484–1497.

- [32] A. Tan, J. Lek, W. Sun, A. Bhowmik, I. Marinescu, X. Song, W. Zhai, F. Li, Z. Dong, C. Boothroyd, E. Liu, Influence of Particle Velocity When Propelled Using N₂ or N₂-He Mixed Gas on the Properties of Cold-Sprayed Ti6Al4V Coatings, *Coatings*. 8 (2018) 327.
- [33] V.N.V. Munagala, V. Akinyi, P. Vo, R.R. Chromik, Influence of Powder Morphology and Microstructure on the Cold Spray and Mechanical Properties of Ti6Al4V Coatings, *J. Therm. Spray Technol.* 27 (2018) 827–842.
- [34] V.N.V. Munagala, S.I. Imbriglio, R.R. Chromik, The influence of powder properties on the adhesion strength and microstructural evolution of cold sprayed Ti6Al4V single splats, *Mater. Lett.* 244 (2019) 58–61.
- [35] V. Satish, B. Kyle, W.J. Grant, Influence of Powder Microstructure on the Microstructural Evolution of As-Sprayed and Heat Treated Cold-Sprayed Ti-6Al-4V Coatings, *J. Therm. Spray Technol.* 28 (2018) 174–188.
- [36] W. Wong, E. Irissou, J.G. Legoux, P. Vo, S. Yue, Powder Processing and Coating Heat Treatment on Cold Sprayed Ti-6Al-4V Alloy, *Mater. Sci. Forum.* 706–709 (2012) 258–263.
- [37] H. Aydin, M. Alomair, W. Wong, P. Vo, S. Yue, Cold Sprayability of Mixed Commercial Purity Ti Plus Ti6Al4V Metal Powders, *J. Therm. Spray Technol.* 26 (2017) 360–370.
- [38] H. Zhou, C. Li, G. Ji, S. Fu, H. Yang, X. Luo, G. Yang, C. Li, Local microstructure inhomogeneity and gas temperature effect in in-situ shot-peening assisted cold-sprayed Ti-6Al-4V coating, *J. Alloys Compd.* 766 (2018) 694–704.
- [39] X. Luo, Y. Wei, Y. Wang, C. Li, Microstructure and mechanical property of Ti and Ti6Al4V prepared by an in-situ shot peening assisted cold spraying, *JMADE*. 85 (2015) 527–533.
- [40] W. Sun, A.W.Y. Tan, N.W. Khun, I. Marinescu, E. Liu, Effect of substrate surface condition on fatigue behavior of cold sprayed Ti6Al4V coatings, *Surf. Coatings Technol.* 320 (2017) 452–457.
- [41] W.Y. Li, C. Zhang, X. Guo, J. Xu, C.J. Li, H. Liao, C. Coddet, K.A. Khor, Ti and Ti-6Al-4V coatings by cold spraying and microstructure modification by heat treatment, *Adv. Eng. Mater.* 9 (2007) 418–423.
- [42] P. Vo, E. Irissou, J.G. Legoux, S. Yue, Mechanical and microstructural characterization of cold-sprayed Ti-6Al-4V after heat treatment, *J. Therm. Spray Technol.* 22 (2013) 954–964.
- [43] N.W. Khun, A.W.Y. Tan, W. Sun, E. Liu, Effect of Heat Treatment Temperature on Microstructure and Mechanical and Tribological Properties of Cold Sprayed Ti-6Al-4V Coatings, *Tribol. Trans.* 60 (2017) 1033–1042.
- [44] C. Chen, Y. Xie, X. Yan, S. Yin, R. Huang, R. Zhao, J. Wang, Z. Ren, M. Liu, H. Liao, Effect of hot isostatic pressing (HIP) on microstructure and mechanical properties of Ti6Al4V alloy fabricated by cold spray additive manufacturing, *Addit. Manuf.* (2019) 1–31.

- [45] M.A. Garrido, P. Sirvent, P. Poza, Evaluation of mechanical properties of Ti6Al4V cold sprayed coatings, *Surf. Eng.* 0 (2017) 1–8.
- [46] ASTM E2109 – 01, Standard Test Methods for Determining Area Percentage Porosity in Thermal Sprayed Coatings, *ASTM Int.* 1 (2014) 1–8. www.astm.org.
- [47] J.R. Santisteban, M.R. Daymond, J.A. James, L. Edwards, IUCr, ENGIN-X: a third-generation neutron strain scanner, *J. Appl. Crystallogr.* 39 (2006) 812–825.
- [48] J.R. Hönnige, P.A. Colegrove, B. Ahmad, M.E. Fitzpatrick, S. Ganguly, T.L. Lee, S.W. Williams, Residual stress and texture control in Ti-6Al-4V wire + arc additively manufactured intersections by stress relief and rolling, *Mater. Des.* 150 (2018) 193–205.
- [49] C. Bühr, B. Ahmad, P.A. Colegrove, A.R. McAndrew, H. Guo, X. Zhang, Prediction of residual stress within linear friction welds using a computationally efficient modelling approach, *Mater. Des.* 139 (2018) 222–233.
- [50] G.S. Pawley, IUCr, Unit-cell refinement from powder diffraction scans, *J. Appl. Crystallogr.* 14 (1981) 357–361.
- [51] M. Nishida, T. Jing, M.R. Muslih, T. Hanabusa, Residual stress measurement of titanium casting alloy by neutron diffraction, in: *AIP Conf. Proc.*, 2008: pp. 101–104. doi:10.1063/1.2906037.
- [52] A.M. Stapleton, S.L. Raghunathan, I. Bantounas, H.J. Stone, T.C. Lindley, D. Dye, Evolution of lattice strain in Ti-6Al-4V during tensile loading at room temperature, *Acta Mater.* 56 (2008) 6186–6196.
- [53] J. Zhang, X. Wang, S. Paddea, X. Zhang, Fatigue crack propagation behaviour in wire+arc additive manufactured Ti-6Al-4V: Effects of microstructure and residual stress, *Mater. Des.* 90 (2016) 551–561.
- [54] M.B. Prime, Cross-Sectional Mapping of Residual Stresses by Measuring the Surface Contour After a Cut, *J. Eng. Mater. Technol.* 123 (2001) 162.
- [55] B. Ahmad, S.O. van der Veen, M.E. Fitzpatrick, H. Guo, Measurement and modelling of residual stress in wire-feed additively manufactured titanium, *Mater. Sci. Technol.* 34 (2018) 2250–2259.
- [56] ASTM E1876 – 15, Standard Test Method for Dynamic Young's Modulus, Shear Modulus, and Poisson's Ratio by Impulse Excitation of Vibration, *ASTM Int.* (2015) 1–17. www.astm.org.
- [57] D. Boruah, X. Zhang, M. Doré, An Analytical Method for Predicting Residual Stress Distribution in Selective Laser Melted/Sintered Alloys, in: *Residual Stress. 2018 – ECRS-10*, *Mater. Res. Proc.* 6, 2018: pp. 283–288.
- [58] P. Mercelis, J. Kruth, Residual stresses in selective laser sintering and selective laser melting, *Rapid Prototyp. J.* 12 (2006) 254–265.
- [59] W.B. Choi, L. Li, V. Luzin, R. Neiser, T. Gnäupel-Herold, H.J. Prask, S. Sampath, A. Gouldstone,

- Integrated characterization of cold sprayed aluminum coatings, *Acta Mater.* 55 (2007) 857–866.
- [60] R. Singh, S. Schrufer, S. Wilson, J. Gibmeier, R. Vassen, Influence of coating thickness on residual stress and adhesion-strength of cold-sprayed Inconel 718 coatings, *Surf. Coatings Technol.* 350 (2018) 64–73.
- [61] Y.C. Tsui, T.W. Clyne, An analytical model for predicting residual stresses in progressively deposited coatings Part 1: Planar geometry, *Thin Solid Films.* 306 (1997) 23–33.
- [62] S. Kuroda, T.W. Clyne, The quenching stress in thermally sprayed coatings, *Thin Solid Films.* 200 (1991) 49–66.
- [63] M. Shiomi, K. Osakadal, K. Nakamural, T. Yamashital, F. Abe, Residual stress within metallic model made by selective laser melting process, *CIRP Ann. - Manuf. Technol.* 53 (2004) 195–198.
- [64] R. Ghelichi, S. Bagherifard, D. Macdonald, I. Fernandez-Pariente, B. Jodoin, M. Guagliano, Experimental and numerical study of residual stress evolution in cold spray coating, *Appl. Surf. Sci.* 288 (2014) 26–33.
- [65] R. Ghelichi, D. MacDonald, S. Bagherifard, H. Jahed, M. Guagliano, B. Jodoin, Microstructure and fatigue behavior of cold spray coated Al5052, *Acta Mater.* 60 (2012) 6555–6561.
- [66] R. Ghelichi, S. Bagherifard, D. Mac, M. Brochu, H. Jahed, B. Jodoin, M. Guagliano, Fatigue strength of Al alloy cold sprayed with nanocrystalline powders, *Int. J. Fatigue.* 65 (2014) 51–57.
- [67] A. Moridi, S.M. Hassani-Gangaraj, M. Guagliano, S. Vezzu, Effect of Cold Spray Deposition of Similar Material on Fatigue Behavior of Al 6082 Alloy, in: Springer, Cham, 2014: pp. 51–57.
- [68] H. Mahmoudi-Asl, The effect of residual stress induced by cold spray coating on fatigue life of magnesium alloy, AZ31B, University of Waterloo, Waterloo, 2011. <https://uwspace.uwaterloo.ca/bitstream/handle/10012/6370/Mahmoudi-Asl?sequence=1> (accessed September 2, 2017).
- [69] C.Y. Jeong, S. Ha, Fatigue properties of Al–Si casting alloy with cold sprayed Al/SiC coating, *Int. J. Cast Met. Res.* 21 (2008) 235–238.
- [70] T. Samson, D. MacDonald, R. Fernandez, B. Jodoin, Effect of Pulsed Waterjet Surface Preparation on the Adhesion Strength of Cold Gas Dynamic Sprayed Aluminum Coatings, *J. Therm. Spray Technol.* 24 (2015) 984–993.
- [71] J. Cizek, M. Matejkova, I. Dlouhy, F. Siska, C.M. Kay, J. Karthikeyan, S. Kuroda, O. Kovarik, J. Siegl, K. Loke, K.A. Khor, Influence of Cold-Sprayed, Warm-Sprayed, and Plasma-Sprayed Layers Deposition on Fatigue Properties of Steel Specimens, *J. Therm. Spray Technol.* 24 (2015) 758–768.
- [72] J. Cizek, O. Kovarik, J. Siegl, K. Aik, I. Dlouhy, Influence of plasma and cold spray deposited Ti Layers on high-cycle fatigue properties of Ti6Al4V substrates, *Surf. Coat. Technol.* 217 (2013)

23–33.

- [73] A. Moridi, S.M. Hassani Gangaraj, S. Vezzu, M. Guagliano, Number of passes and thickness effect on mechanical characteristics of cold spray coating, *Procedia Eng.* 74 (2014) 449–459.

ACCEPTED MANUSCRIPT

Tables

Table I: Chemical compositions (mass %) of Ti-64 powders and mill annealed Ti-64 substrate material

Powder, substrate	Ti	Al	V	Fe	O	Si	Sn	Cr	Ni	Others
Ti-64 powder (15-32 μm)	Balance	6.48	4.03	0.17	0.17	0.01	0.02	<0.01	<0.02	<0.01
Mill annealed Ti-64	Balance	6.32	4.16	0.20	0.13	0.02	<0.01	0.02	0.01	<0.01

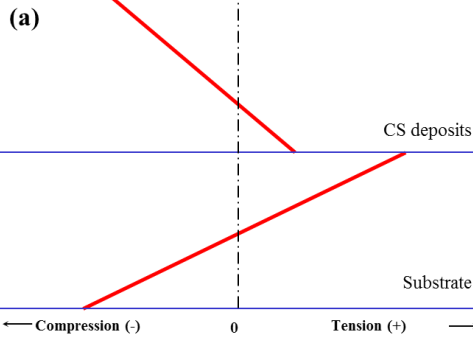
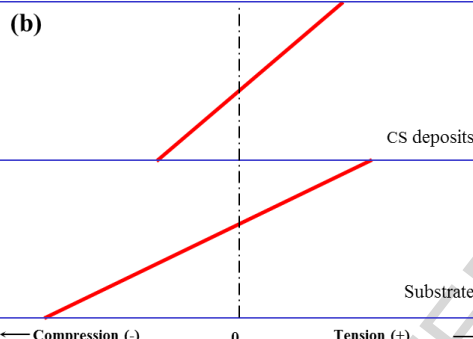
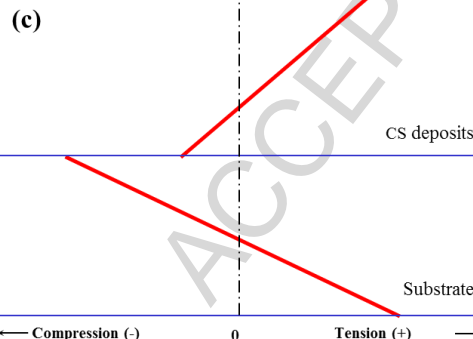
Table II: Cold spray process parameters

Process gas	N ₂
Gas pressure (MPa)	5
Gas temperature (°C)	1100
Scanning speed (mm/s)	500 and 300 (see Table III)
Track spacing (mm)	2
Spray angle (°)	90
Standoff distance (mm)	30
Track pattern	Horizontal track and cross-hatch track pattern (see Figure 2)
Surface preparation	Ground with 120 alumina grit and cleaned using ultrasonic bath

Table III: Specimen details for residual stress measurements

Specimen name	Substrate thickness (mm)	No. of layers	Coating thickness (mm)	Track pattern	Average layer thickness (μm)	Length, width (mm)	Scanning speed (mm/s)
CS1	5	42	4.5	Horizontal	~107	60, 30	500
CS2	5	14	1.5	Horizontal	~107	60, 30	500
CS3	5	14	1.5	Cross-hatch	~107	60, 30	500
CS4	5	8	1.5	Horizontal	~187	60, 30	300
CS5	10	14	1.5	Horizontal	~107	60, 30	500
CS6	5	0	0	-	0	60, 30	-

Table IV: Different residual stress profiles in cold sprayed deposit-substrate assemblies resulting from different stress build-up mechanisms.

Residual stress profile	Deposit/substrate assembly (examples)	Process gas, pressure and temperature	Residual stress build-up mechanism
 <p>(a)</p> <p>CS deposits</p> <p>Substrate</p> <p>← Compression (-) 0 Tension (+) →</p>	Cu/Cu, Cu/Al [12]	He at 0.62 MPa 140°C	Type A: Peening dominant CS process
	Al/Al, Al/Cu [12]	He at 0.62 MPa and 200°C	
	Al/Al [59]	He at 1.72 MPa and 325°C	
	Al/Mg [13]	He at 0.62 MPa and 77-132°C, N ₂ at 0.76 MPa and 217°C	
	Al6061/Mg, Al7075/Mg [13]	N ₂ at 3.85 MPa and 400°C	
 <p>(b)</p> <p>CS deposits</p> <p>Substrate</p> <p>← Compression (-) 0 Tension (+) →</p>	Ti/Cu [14]	He at 0.62 MPa and 365°C N ₂ at 3.9 MPa and 615°C	Type B: Thermal mismatch dominant CS process
	Ti/Fe [14]	Not available	
	Al/Mg [13]	N ₂ at 3.85 MPa and 550°C	
 <p>(c)</p> <p>CS deposits</p> <p>Substrate</p> <p>← Compression (-) 0 Tension (+) →</p>	Ti-64/Ti-64 (this study)	N ₂ at 5 MPa and 1100°C	Type C: High thermal gradient and quenching dominant CS process

List of figure captions

Figure 1: Characteristics of the Ti-64 powder: (a) particle size distribution, (b) powder morphology, (c) microstructure of as received powder showing the rapidly solidified α' martensitic needles.

Figure 2: CS track patterns: (a) horizontal track pattern, (b) cross-hatch track pattern

Figure 3: SEM microstructure showing: (a) CS deposits, substrate and the interface, the dark areas in the coating are process induced defects; (b) CS deposits consisting of ‘textured’ and ‘smooth’ regions.

Figure 4: (a) Specimen CS1 used for residual stress measurement by neutron diffraction method, (b) stress-free (d_0) specimen extracted from the centre of a CS deposited specimen using WEDM, and (c) experimental set-up at the ENGINE-X, ISIS. Note: stress components in the X, Y, and Z directions are referred to as normal, transverse, and longitudinal stresses, respectively.

Figure 5: Exemplary fitted spectra for three orthogonal directions (normal, transverse, and longitudinal), taken from a measurement point in the CS deposits of specimen CS1.

Figure 6: (a) specimen CS2 showing the cutting plane at the mid-length of the specimen; (b), (c), cut surfaces of the specimen after WEDM cutting. Note: stress component of interest is in the Z direction and referred to as the longitudinal stress

Figure 7: Impulse excitation set-up for Young’s modulus (E) measurement.

Figure 8: Residual stress distributions along the thickness direction of the three orthogonal stress components (normal, transverse, and longitudinal), measured by neutron diffraction.

Figure 9: (a) Two-dimensional residual stress maps produced by the contour method on the X-Y plane (longitudinal stress component) for all six specimens (refer Table III); (b), (c), (d), averaged stresses in the X-Y plane for comparison among the specimens.

Figure 10: Build-up of residual stresses by high thermal gradient and quenching dominant CS process that uses very high process gas temperature and pressure: residual stress distribution due to the stress induced by deposition of (a) one layer [57], (b) two layers, (c) three layers, and (d) ‘ n ’ layers [57].

Figure 11: Comparison of residual stress distributions (longitudinal stress component) among neutron diffraction, contour method, and analytical prediction (specimen CS1).

Figures

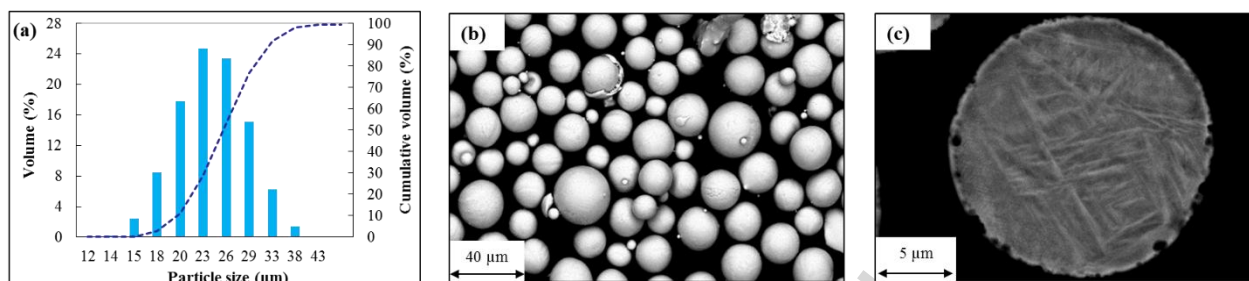


Figure 1

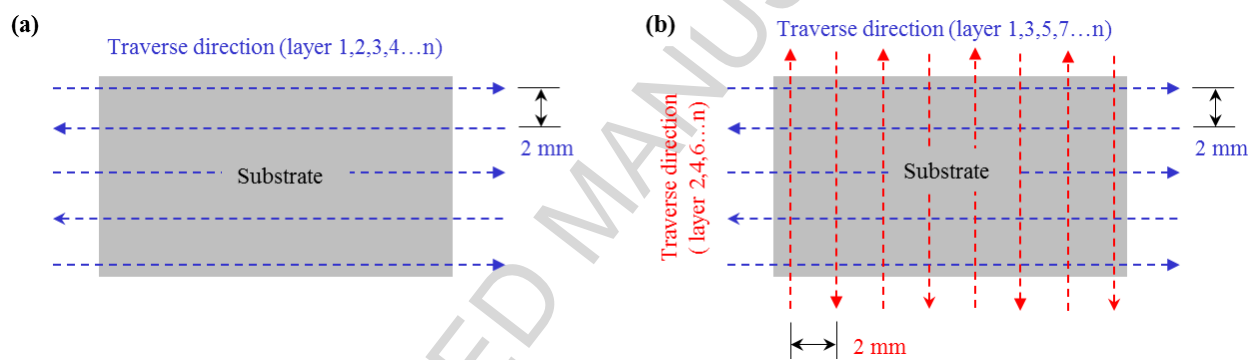


Figure 2

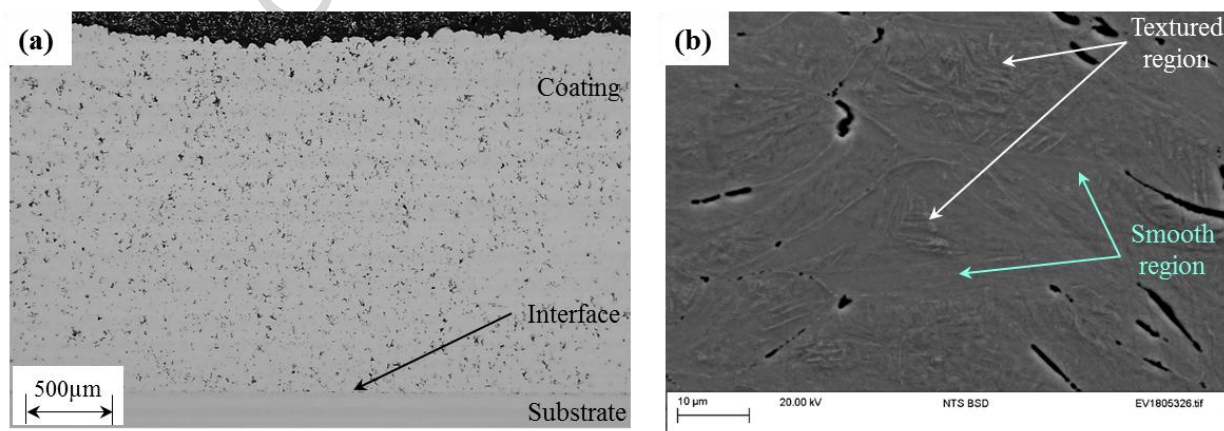


Figure 3

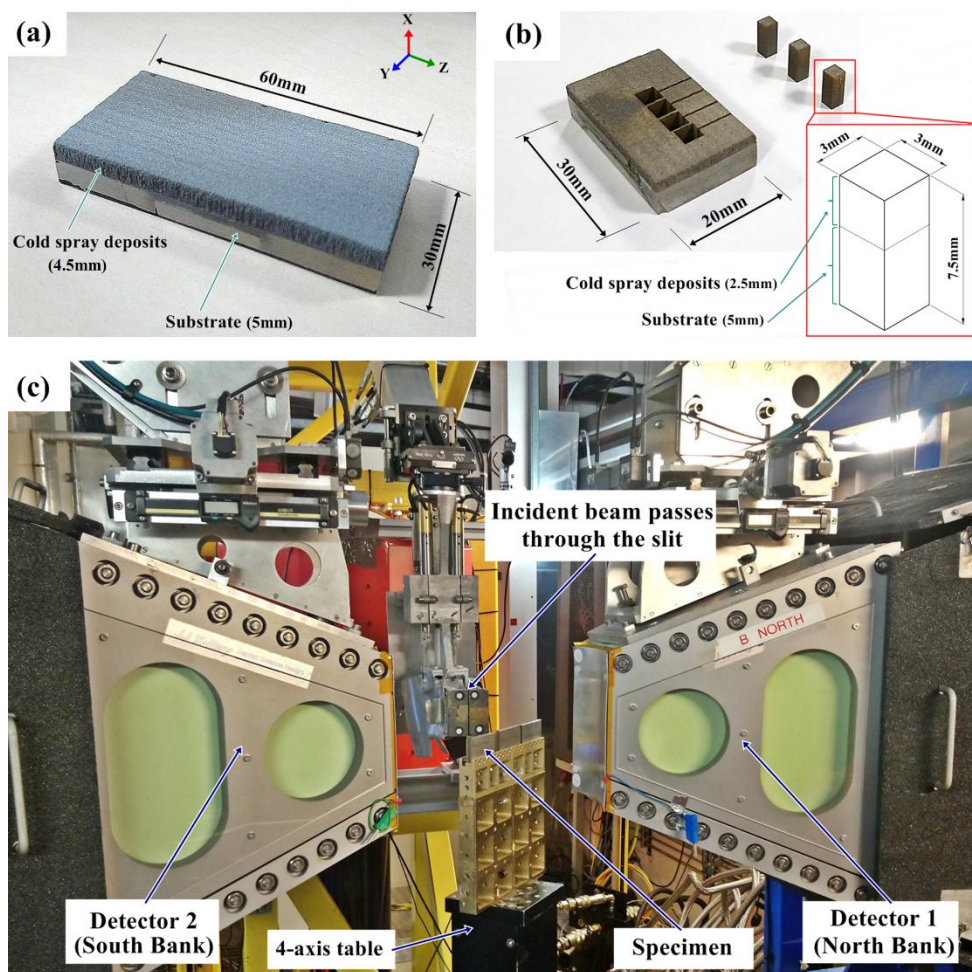


Figure 4

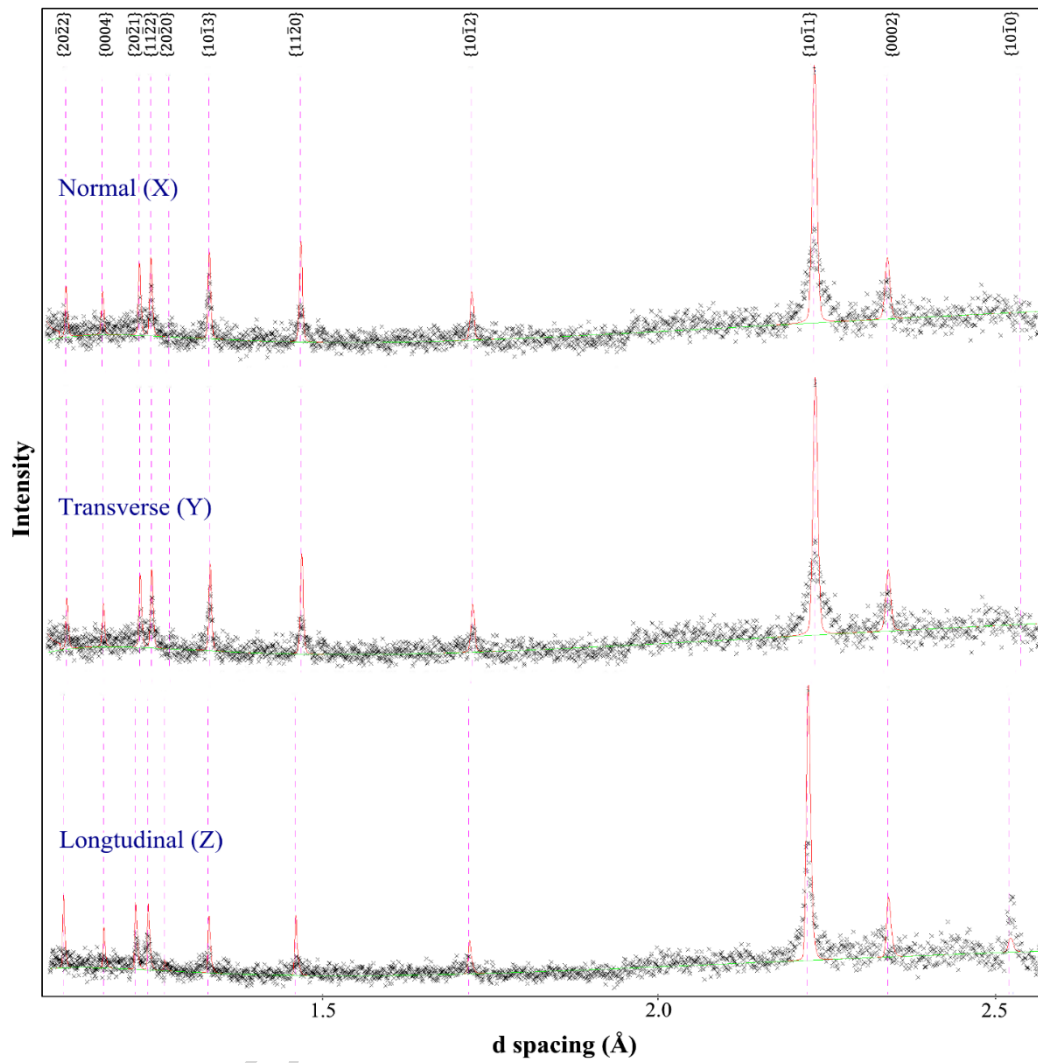


Figure 5

ACCEP

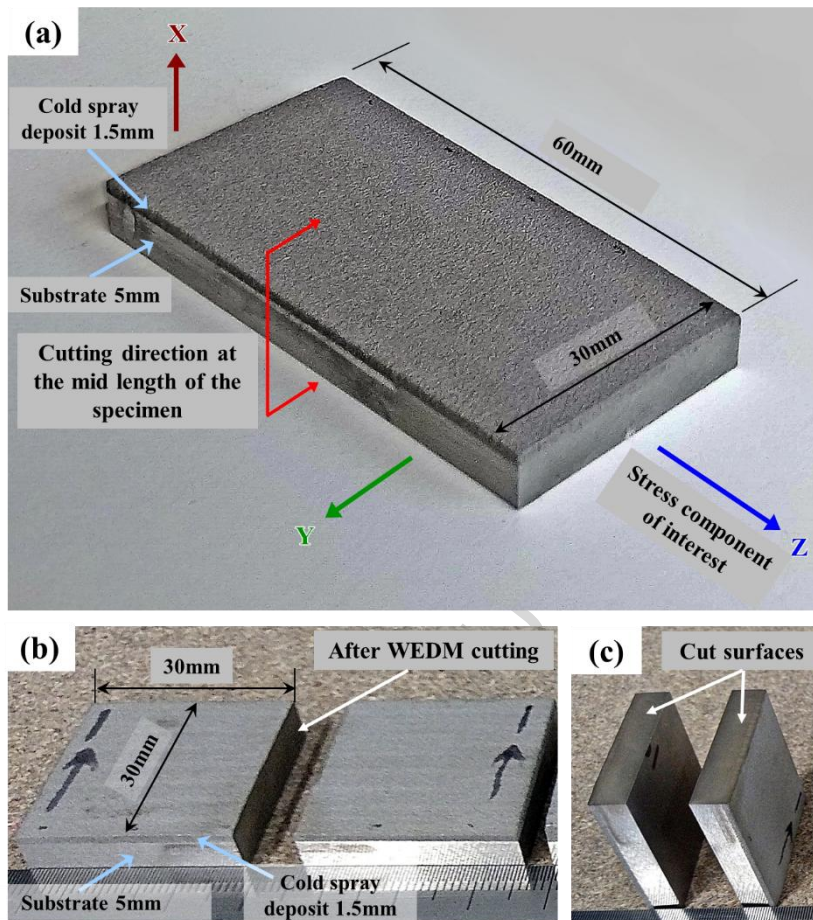


Figure 6

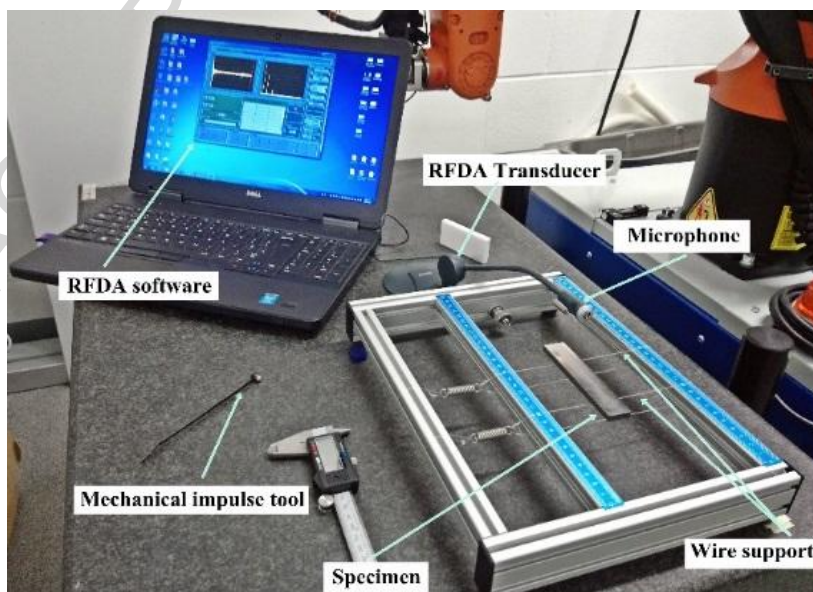


Figure 7

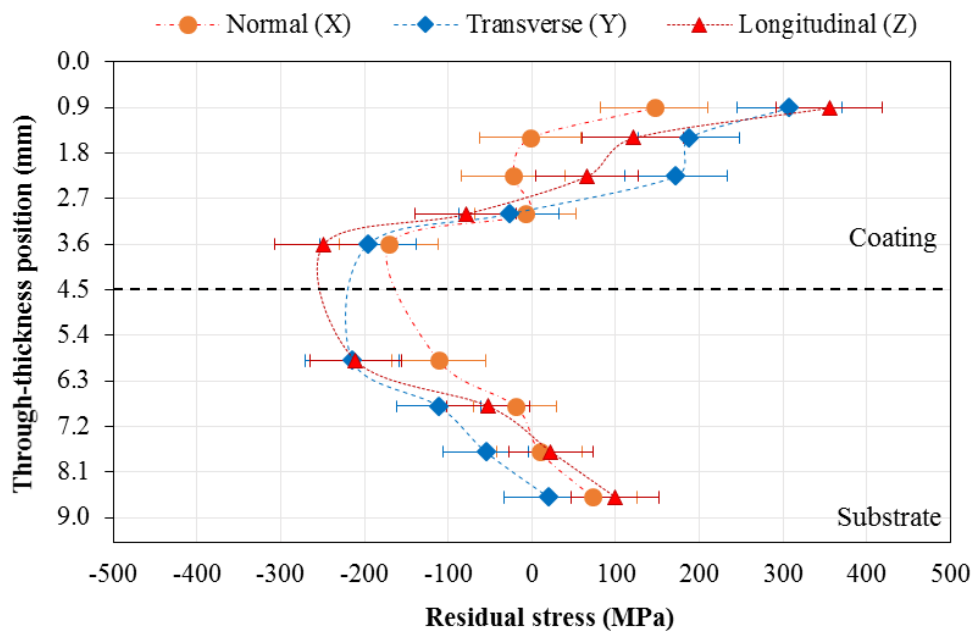


Figure 8

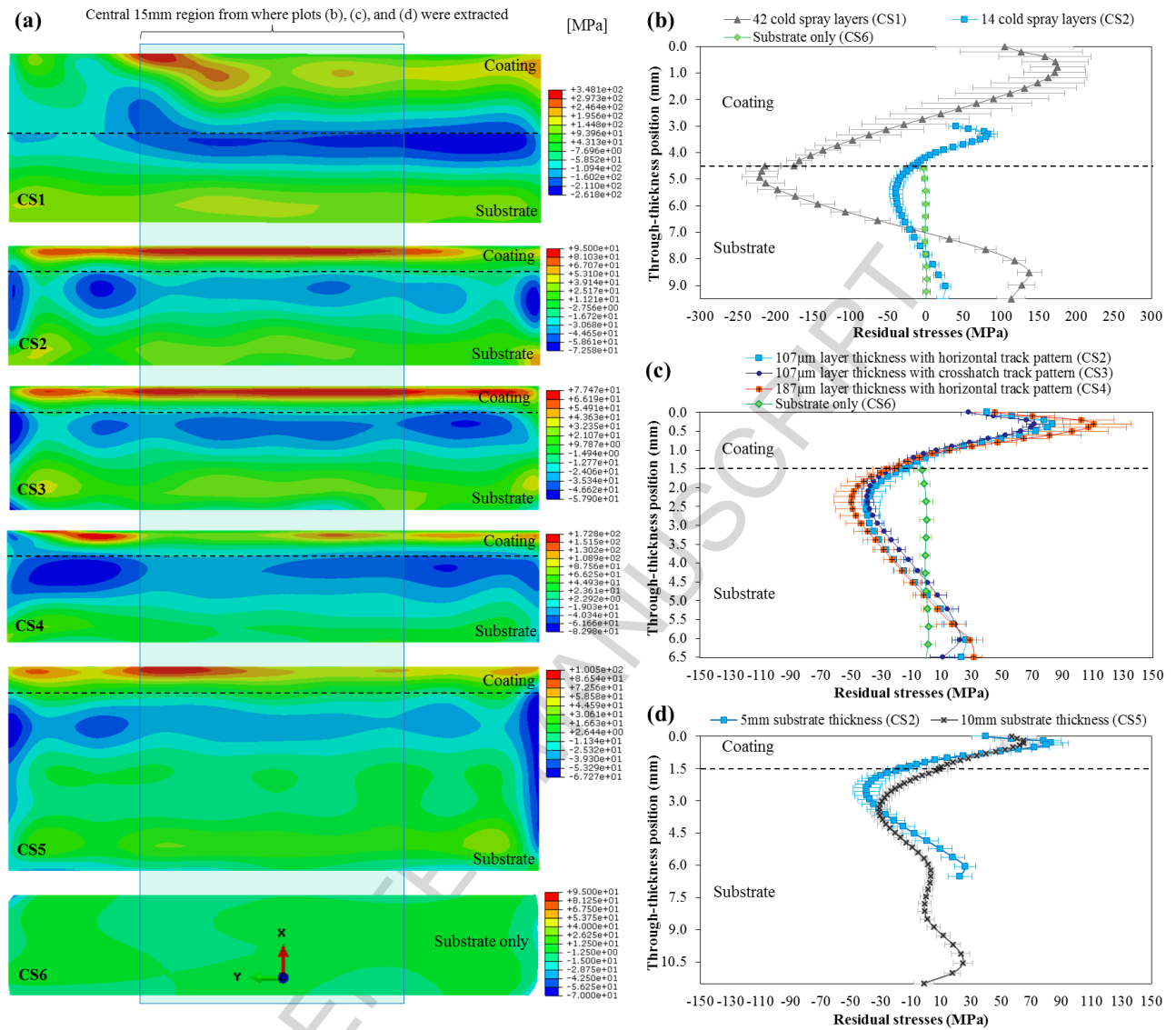


Figure 9

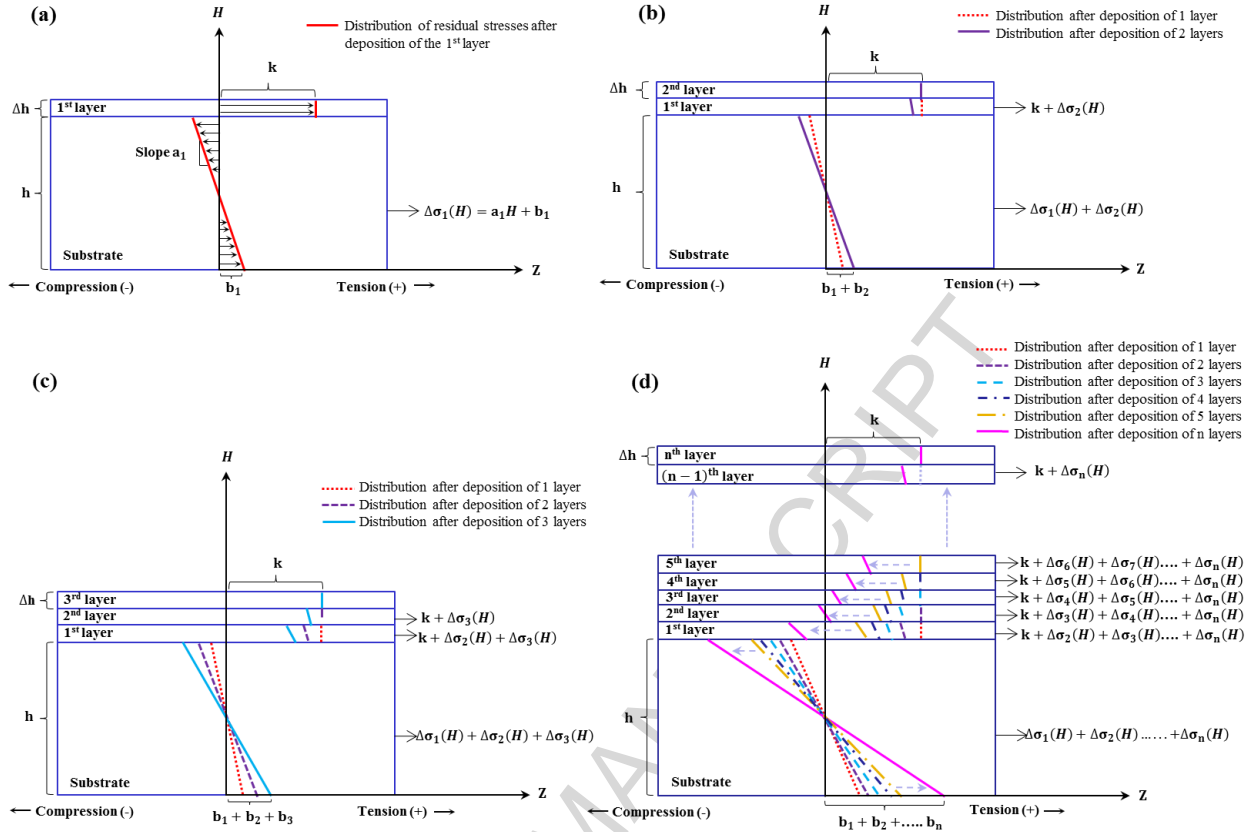


Figure 10

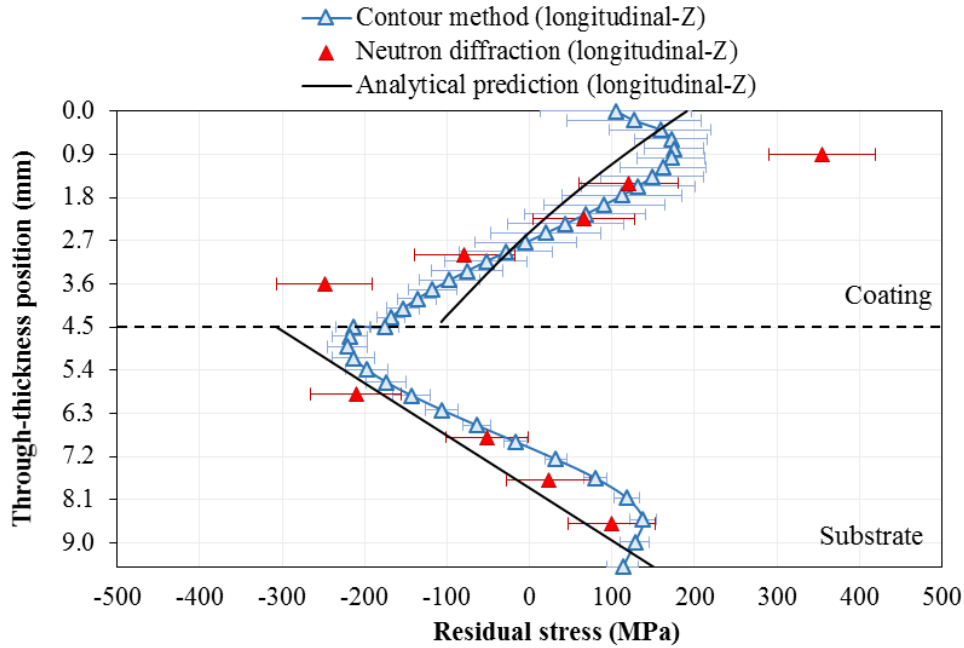


Figure 11

Highlights

- Residual stresses induced by cold spraying of Ti-6Al-4V on Ti-6Al-4V substrates were evaluated using the neutron diffraction method and the contour method.
- An analytical method was used to interpret the experimental results and to study different residual stress build-up mechanisms induced by the cold spray process.
- A parametric study was carried out on the effect of geometrical variables, scanning speed and track pattern on the distribution and magnitude of residual stresses.